Shear-Force Sensor With Point-Symmetric Electrodes Driven by LTPS TFT Active Matrix Backplane

Noriyuki Kawashima, Tomohiro Sampei, Takuro Tanaka, Daiki Suzuki, Kazunori Morita, Miya Yoshimoto, and Katsuyoshi Hiraki

***Abstract*—In this study, we successfully demonstrated a 700 μm thick shear-force sensor with 60 $\times$ 60 high resolution array by introducing a combination of an originally developed pressure-sensing elastomer and a newly proposed taxel (tactile pixel) structure with four point-symmetric electrodes. When shear forces are applied to the sensor substrate in several directions by lifting a weight, four sets of resistances between the electrodes are read through low-temperature polycrystalline-silicon (LTPS) thin-film transistors (TFTs) in each taxel and clear outputs corresponding to that direction can be confirmed. Furthermore, as a result of evaluating the object recognition performance of the tactile sensor by using jigs with engraved small dimples, it was confirmed that the recognized minimum size of the shape was 1.5 mm, which suggests that the spatial resolution of this sensor is superior to the human hand perception ability. Because this sensor is ultra-thin, not bulky, and potentially applicable to flexible substrates, it is quite promising as a sensor that can be mounted on the fingertip of a robot hand with multiple functions.**

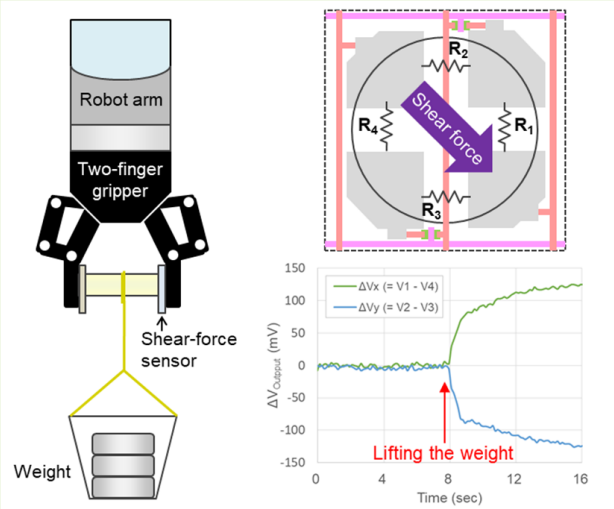

***Index Terms*—Tactile sensor, pressure sensor, shear-force sensor, thin-film transistors, pressure sensing elastomer.**

I. Introduction

FOR many years, articulated robot arms have been utilized for a wide variety of industrial applications, such as welding processes, semiconductor wafer and LCD panel transfer, electronic parts implementation, and biomedical related processes. However, these types of robot arms are fully customized and limited to a single task in many cases; thus, a robot hand designed to imitate the human hand function must be more suitable for multiple complex tasks. To improve the accuracy of robotic hand manipulation and object grasping, a more sensitive, precise, and multi-functional tactile sensing device is necessary.

Kamiyama *et al.* demonstrated a tactile sensor called GelForce, which contains an imaging device and transparent silicon rubber. When an object contacts the tactile sensor surface, a two-layered marker pattern inside the silicone rubber deforms and is translated into the topographic information of the contacted material [1]. MIT groups reported a unique tactile sensor combining a gel elastomer and vision camera system, which can be mounted on the fingertip of a robot hand and can capture 3D height maps of grasped objects [2], [3]. Yamaguchi *et al.* reported a vision-based tactile sensor that is attached to a robot hand for more practical applications, such as cutting vegetables using a knife. By monitoring the three-axis (x, y, z) applied force at a high frame rate, the sensor offers precise information of grasping conditions and helps to prevent slippage of the knife [4]. As described, many vision-based tactile sensors have been reported; however, because of their bulky structure, it is difficult to place them on the fingertip of a robot hand developed for multi-tasking.

Compared to vision-based tactile sensors, thin-film transistor-based tactile sensors are more advantageous in terms of thickness, scalability, multi-function integration, and flexibility. Someya *et al.* demonstrated a flexible active matrix pressure sensor with 32 $\times$ 32 sensing cells (SENCEL) by combining an organic thin-film transistor (OTFT) array on a

Manuscript received October 6, 2021; accepted December 17, 2021. Date of publication December 29, 2021; date of current version February 11, 2022. The associate editor coordinating the review of this article and approving it for publication was Dr. Eui-Hyeok Yang. *(Corresponding author: Noriyuki Kawashima.)*

The authors are with the Advanced Technology Research Department, LG Japan Lab Inc., Tokyo 140-0002, Japan (e-mail: noriyuki.kawashima@lgjlab.com).

Digital Object Identifier 10.1109/JSEN.2021.3139067

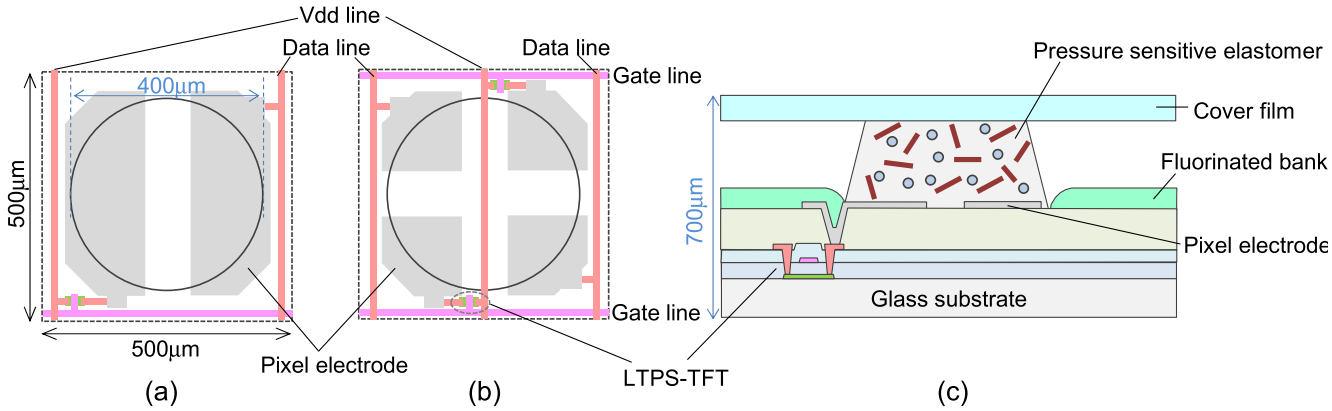

Fig. 1. Cell structure of 1Tr-1R type pressure sensor (a) and 2Tr-4R type shear-force sensor (b). Schematic cross-sectional view of both sensor substrates (c).

PEN substrate and pressure-sensitive rubber [5]. Furthermore, they reported a double-function organic-based sensor array with a pressure sensor and a thermal sensor that employs a heterojunction of p-type and n-type organic semiconductors [6].

In addition to pressure sensing and topography detection, shear-force sensing is essential for the slip detection function of robotic hand applications to secure object grasping, as mentioned above. Various types of piezoresistive shear-force sensors have been fabricated by constructing microelectromechanical systems (MEMS)-based structures on rigid or flexible substrates [7]–[11]. Oh *et al.* applied a new type of dual-gate zinc oxide (ZnO) TFT to demonstrate the rough resolution of tactile and shear-force sensors [12]. In contrast, shear-force sensing arrays have been demonstrated using a capacitance detection method with a combination of floating electrodes with an inserted low-modulus elastic rubber or an air gap between them [13]–[16]. Shear-force sensors using optical mechanisms have also been proposed [17]–[19]. In some cases, these types of optical sensors are not compatible with mounting on the robotic hand and require a complex analytical scheme to quantify the applied shear force.

In this study, we have reported the basic operation demonstration of a shear force sensor, which possesses a new operating principle. It is a non-piezoresistive, non-capacitive, and non-optical shear-force and pressure sensor. As it is an ultra-thin, highly scalable, simple structure that is potentially applicable to high-resolution and flexible sensors, it can contribute to the high-precision sensing of multitasking robots that can perform complicated tasks.

II. Cell Design and Working Mechanism

We designed two types of sensor cell structures, which consist of a one transistor–one resistance (1Tr-1R) structure for pressure detection and a 2Tr-4R structure for shear-force detection. Figure 1(a) and (b) show the schematics of the 1Tr-1R type pressure sensor cell and 2Tr-4R type shear-force sensor cell, respectively. In both types of cells, the centered circle indicates the patterned area of the pressure-sensitive elastomer. As shown in Figure 1(c), a pressure-sensitive elastomer was patterned on the taxel electrodes of the LTPS-TFT backplane. The pressure-sensitive elastomer consists of an ultra-low modulus silicone elastomer with a uniform dispersion of conductive filler materials, such as Ni and titanium dioxide (TiO_2). Despite the space limitation of the 500 μm $\times$ 500 μm sensor cell, the taxel electrode was designed to be as large as possible for reliable ohmic contact between the minute filler materials and taxel electrodes. On the LTPS-TFT backplane, a fluorinated bank was patterned by photolithography to improve the patterning accuracy of the dispensed conductive elastomers, resulting in more uniform electrical properties. A cover film with a sufficiently high Young's modulus should be selected so that most of the applied pressure can be transmitted to the sensor effectively without deforming the cover film or dispersing the applied pressure. Accordingly, more sensitive detection can be achieved. Furthermore, a cover film is necessary to protect the pressure-sensitive elastomer from the damage caused by nail scratching or rough-surface objects.

Figure 2 shows the working mechanism of the pressure sensor (a) and the shear-force sensor (b). When vertical pressure is applied to the 1Tr-1R type pressure sensor, the elastomer is compressed, and the average distance between adjacent conductive filler materials is shortened, resulting in lower resistance (R) between the two distanced taxel electrodes. The changed resistance value during this process is transferred to the external ADC circuits through the taxel TFT and converted into the numerical information of the applied pressure. In contrast, when shear force is applied to the 2Tr-4R type sensor, the elastomer deforms laterally, as shown in Figure 2(b), and the distance between the filler materials decreases only in the direction in which the shear force is applied, resulting in decreased resistance (R_1). Thus, the shear direction is determined. Analysis using an in-depth algorithm is required to calculate the accurate applied shear-force value and direction.

III. Device Fabrication Process

The full process of sensor substrate fabrication is shown in Figure 3(a). First, we fabricated a coplanar top-gate LTPS TFT on a 370 mm $\times$ 470 mm glass substrate. Normally, indium tin oxide (ITO) is used for the taxel electrodes of TFT devices; however, the MoTi/ITO stack is adopted for this sensor device, taking into account the stable ohmic contact between the taxel electrodes and the filler materials. Then,

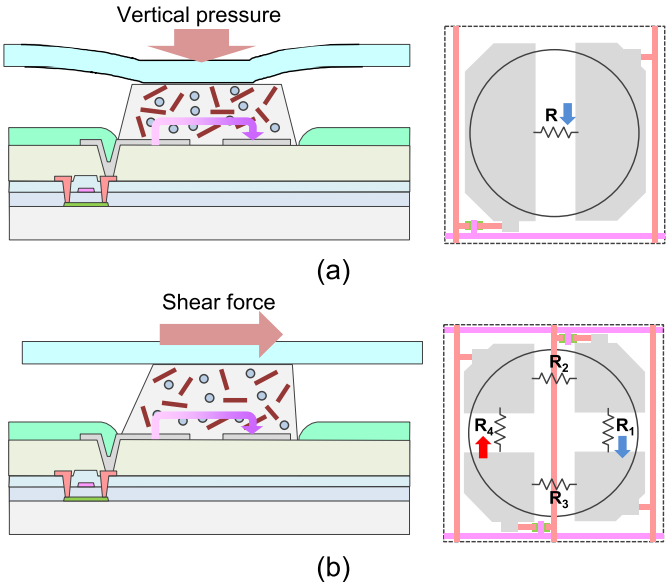

Fig. 2. (a) Schematic cross-sectional view of the 1Tr-1R type pressure sensor when vertical pressure is applied. (b) Schematic cross-sectional view of the 2Tr-4R type shear-force sensor when shear force is applied.

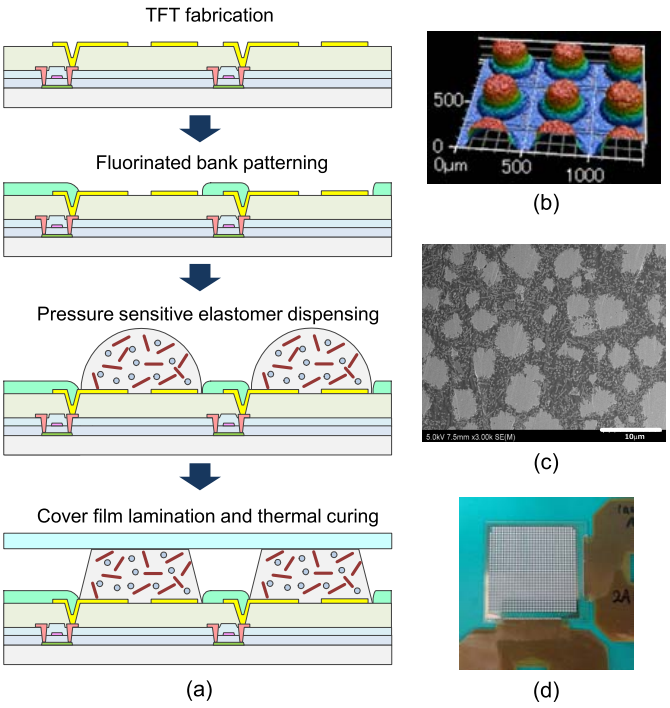

Fig. 3. (a) TFT tactile sensor array fabrication process. (b) 3D topological view of patterned elastomers obtained by a laser scanning microscope. (c) SEM cross-sectional view of the conductive filler containing elastomer. (d) Completed tactile sensor array (60 × 60).

a 20-nm-thick, 400 μm-diameter fluorinated bank layer was patterned by a photolithography process. After completion of the TFT process, the large TFT substrate was cut into small pieces of sensor panels (36 mm × 36 mm). The formulation of the pressure-sensitive elastomer consisted of a heat-curable, dual-component silicone resin (KE-109E A/B, Sin-Etsu Silicones), nickel powder (Type123, Vale), and titanium dioxide (Ishihara Sangyo). After uniformly mixing this formulation, it was carefully dispensed on each circular bank-patterned

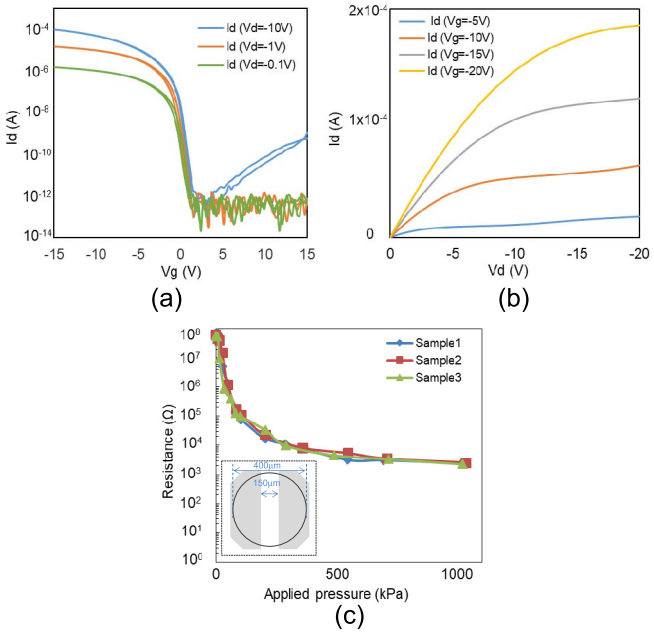

Fig. 4. (a) Transfer characteristics and (b) output characteristics of p-type LPTS TFT. (c) The pressure sensitive elastomer resistance as a function of applied pressure with three samples.

area of the TFT substrate by a screw dispenser (Screw Master 3, Musashi Engineering) on account of the relatively high viscosity and thixotropy of the dispensed paste. While precisely controlling the gap with spacers, the cover film and rigid glass substrate were simultaneously laminated on the elastomer-dispensed TFT surface to create a trapezoid shape of the elastomers [Figure 3(b)]. It was sintered at 150 °C for 2 h for thermal curing of the silicone elastomers, and then the rigid glass substrate was removed. Figure 3(c) shows the SEM image of the cross-sectional view of the fully cured conductive filler containing the elastomer. Finally, a flexible printed circuit (FPC) film was attached to the gate/data pad electrodes of the TFT substrate, and a 60 × 60 tactile sensor array was completed (Figure 3(d)).

IV. Experimental

To ensure accurate and highly sensitive operation of the tactile sensor, we performed a circuit simulation based on the basic TFT characteristics and electrical properties of pressure-sensitive elastomers before designing the taxel structure and external circuit configurations.

A. TEG Device Evaluation and SmartSpice Simulation

Figure 4(a) and (b) show the transfer and output characteristics of the p-type LTPS TFT, respectively. We measured the basic characteristics of the TEG TFT to extract the device parameters applied to the SmartSpice circuit simulation [20]. The TFT channel length was 4 μm and the channel width was 3 μm.

The calculated saturation mobility of the TFT was 60 cm^2/Vs and the threshold voltage was −0.4 V. In parallel, we fabricated a simple TEG device with taxel electrodes and pressure-sensitive elastomers patterned on a glass substrate to evaluate the range of resistance change as a function of applied pressure. A total of three samples were tested to

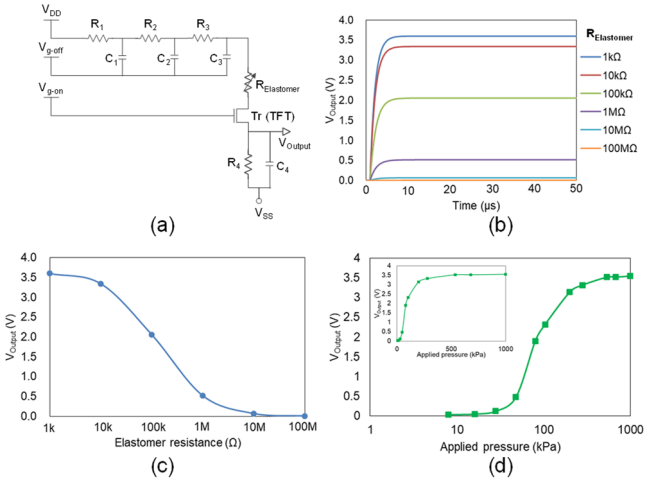

Fig. 5. (a) Simplified circuit diagram of the 1Tr-1R type pressure sensor used for the SILVACO SmartSpice simulation. (b) Simulated output voltage as a function of the elastomer resistance and time after Vg-on is applied. (c) Output voltage as a function of the elastomer resistance. (d) Output voltage as a function of the applied pressure.

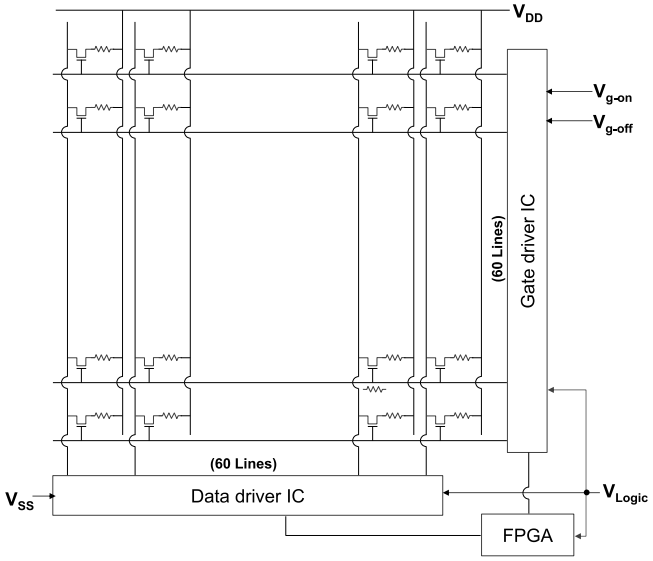

Fig. 6. Schematic diagram of 1Tr-1R type pressure sensing TFT array (60 × 60) with driver circuits.

validate the uniformity of the electrical characteristics of the pressure-sensitive elastomers [Figure 4(c)]. By optimizing the formulation of conductive filler materials and silicone resin, resistance changes of almost five orders of magnitude were obtained for a wide range of applied pressures (0–1,000 kPa). The gap between the taxel electrodes was fixed at 150 μm, as shown in the inset of Figure 4(c). The vertical force was applied using a digital force gauge (ZTS-5N, IMADA, Inc.), and the electrical current flowing through the elastomer was measured using a source/measure unit (B2901A, Keysight Technologies) and then converted to the resistance value.

Both the TFT and pressure-sensitive elastomer characteristics described above were reflected in the SmartSpice simulation. Figure 5(a) shows a simplified circuit diagram for reading the elastomer resistance ($R_{Elastomer}$) as the output voltage through the taxel TFT. R_1–R_3 and C_1–C_3 indicate the parasitic

resistance and parasitic capacitance, respectively. C_4 is AD converter sampling capacitance (30 pF). R_4 is the resistance added to the external circuit, which is important for adjusting the time decay of the output voltage by setting an appropriate ratio of $R_{Elastomer}$ and R_4. Figure 5(b) shows the time decay of the output voltage with a series of elastomer resistances (1k–100 MΩ). These ranges of resistance correspond to the measured actual resistance values of the elastomer. We successfully confirmed that all decays saturated within 10 μs, which is attributed to the relatively higher mobility of LTPS TFT devices, proving that this sensor shows a sufficiently quick response considering the 100 Hz operation of the 60 × 60 array sensor. By combining the time decay of V_{Output} [Figure 5(c)] and the applied pressure dependence of the elastomer resistance [Figure 4(c)], V_{Output} decay as a function of the logarithm of applied pressure was obtained (Figure 5(d)). The inset of Figure 5(d) shows a linear plot of V_{Output} versus applied pressure. Compared to a commercialized resistive-type pressure sensor [21], the linearity of the output voltage versus the applied pressure is insufficient. This could be improved by adjusting the external circuit or by optimizing the TFT resistance.

B. Pressure Sensing Characteristics of 1 Tr-1R Sensor

We successfully simulated the normal operation of the pressure sensor using an actual TFT device and pressure-sensitive elastomer characteristics. Hence, a 60 × 60 tactile sensor array and an external circuit configuration were designed, as shown in Figure 6.

To avoid damage to the TFT devices by electrostatic discharge (ESD), ESD protection diodes were added to each line between the gate driver and the array (not shown in Figure 6). The taxel electrode dimensions were the same as those shown in Figure 4(c). Figure 7 shows actual 2D and 3D pressure mapping when pressure was applied to the sensor with a digital force gauge. The pressing jig diameter was 12 mm. Although the maximum range of this pressure sensor was 1,000 kPa, we initially attempted a relatively lower pressure application to monitor the sensor reaction behavior with gradually increasing pressure. In the "low pressure setup," a 12-bit ADC digital value range from 0 to 4095 was assigned to the output voltage corresponding to the pressure range from 0 to 50 kPa. As a result, the shape of the pressing jig was clearly recognized and we confirmed a gradual transition of pressure mapping images in the relatively smaller steps of applying pressure. Figure 7(c) shows the output voltage versus the applied pressure with two different voltage setups to measure the lower pressure range, as described above, and the higher pressure range. As shown in Figure 7(c), each setup has been tested twice and high reproducibility of the testing data has been confirmed. Although, the deviation of the data was within ±5%, the influence of the applied pressure variation of the pressing jig is considered more dominant than the variation in the sensor itself. The obtained data show that this pressure sensor is potentially applicable to various scenarios without any change of the pressure-sensitive elastomer material itself and the external circuit.

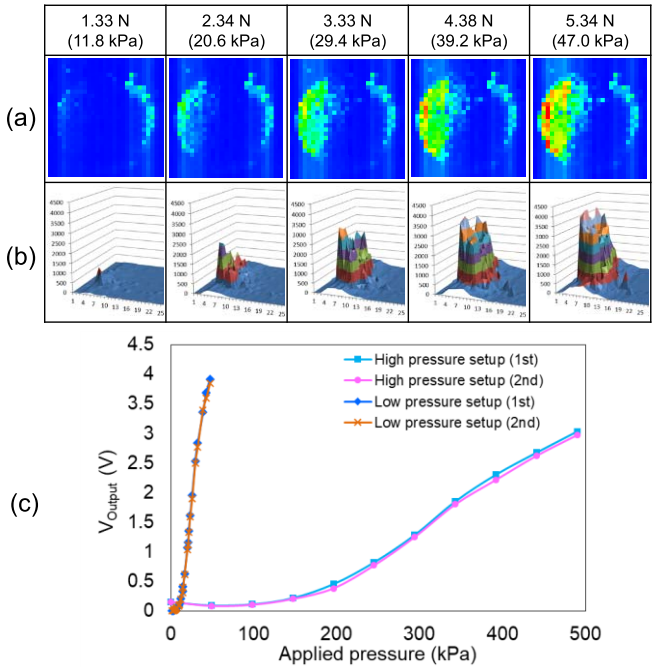

Fig. 7. (a) 2D and (b) 3D pressure mapping images measured by the 1Tr-1R type pressure sensor. (c) Measured V_{Output} as a function of applied pressure with two different setups. 1st and 2nd trials are plotted.

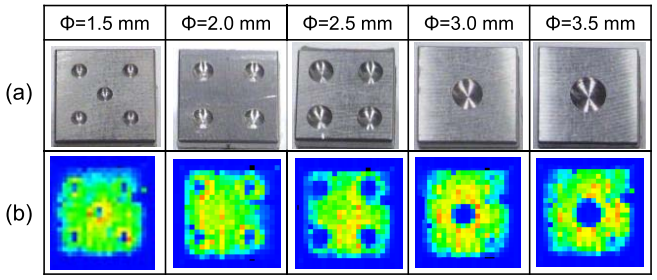

Fig. 8. (a) Stainless steel dice-like jig for object recognition test and (b) the test result.

Among several types of robotic tactile perception, object recognition is regarded as a key problem and has become a major research direction [22]. To evaluate the object recognition performance of the proposed sensor, we prepared a series of stainless steel dice-like jigs with different sizes of engraved dimples, as shown in Figure 8(a). When the jig was pressed on the sensor surface at a relatively higher pressure (>500 kPa), we successfully confirmed that the recognized minimum size of the dimple was 1.5 mm [Figure 8(b)]. Considering that the limit value of two-point discrimination by human fingertips is 2–4 mm [23], it is suggested that the spatial resolution of this sensor is superior to the human hand perception ability. In addition, this resolution could potentially reach a sub-millimeter order if the taxel size is minimized to 100–200 μm, assuming that the paste with a high thixotropic property could be uniformly patterned in such a smaller taxel.

C. Shear-Force Sensing Characteristics of 2Tr-4R Sensor

Figure 9 shows the circuit diagram of the 2Tr-4R type of 60 × 60 shear-force sensor array. The sensor driving scheme is

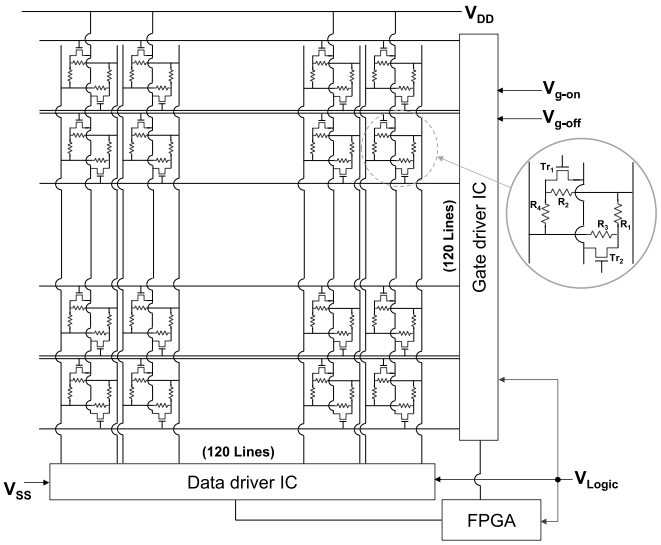

Fig. 9. Schematic diagram of 2Tr-4R type shear-force sensing TFT array (60 × 60) with driver circuits.

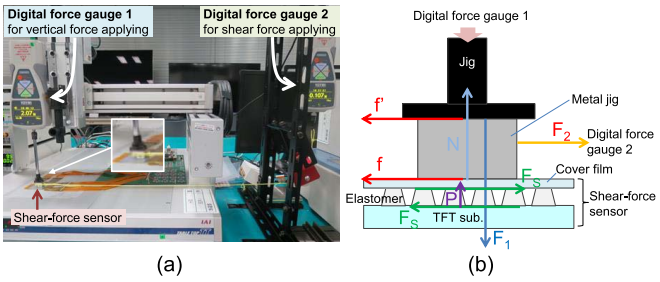

Fig. 10. (a) Typical experimental setup and (b) schematic diagram of the applied forces when evaluating the shear force sensing performance by using a two-set digital force gauge and a three-axis robot.

the same as that of the 1Tr-1R type sensor (Figure 6). In total, four sets of resistances (R_1 to R_4) can be read through two TFTs in each taxel, as shown in the inset of Figure 9. As with the 1Tr-1R cell, the electrode gap was fixed at 150 μm as the optimized gap.

Figure 10(a) shows the basic experimental setup that was used to evaluate the shear-force sensing performance by employing two sets of a digital force gauge and a three-axis robot. The position of each part was precisely adjusted so that one digital force gauge applied pressure in a completely vertical manner and the other digital force gauge applied shear force completely horizontally. Figure 10(b) shows a schematic of the vertical pressure and shear force applied to the shear force sensor by the jig, where static friction exists between the jig and the sensor. The vertically applied force is summarized by equations (1) and (2), where F_1 is the force applied by digital force gauge 1, N is the normal force, P is the compressive force, σ is the compressive pressure on the elastomer, A is the cross-sectional area of the metal jig, ε is the normal strain, and E is the elastic modulus of the elastomer.

$$F_1 = N + P \tag{1}$$

$$\sigma = \frac{P}{A} = \varepsilon E \tag{2}$$

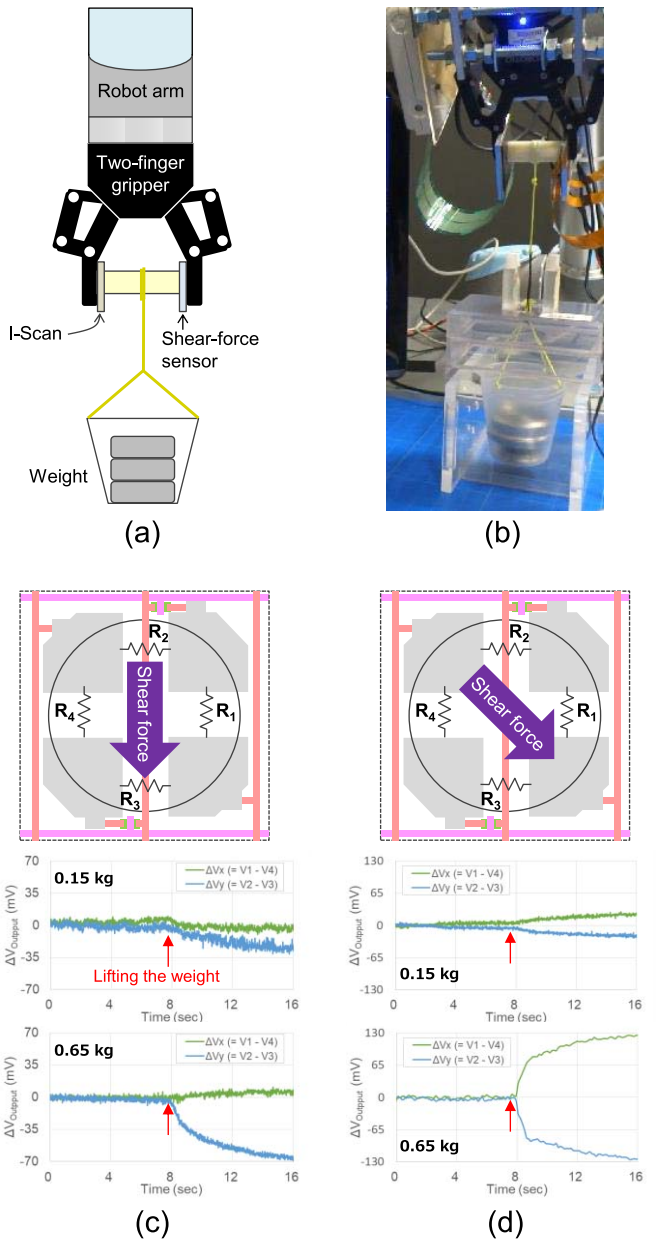

Fig. 11. (a) Schematic and (b) actual image of an experimental setup using a robot hand to lift a weight with a jig sandwiched between two tactile sensors, I-Scan, and a shear force sensor. (c) Time decay of ΔVx and ΔVy when 0.15 and 0.65 kg shear forces are applied consecutively in the downward direction and (d) in the diagonal 45° direction.

The optimization of elastic modulus E of the pressure - sensitive elastomer is quite important in this sensor. This is because, if the elastomer is excessively deformed when grasping the object, the amount of signal change when the shearing force is applied is limited. In contrast, if the elastic modulus is too large, the elastomer will not be deformed; thus, a sufficient value of ΔV_{Output} cannot be obtained.

Regarding the horizontal direction, the force pulled by the other digital force gauge and the two static frictions are balanced, as shown in equations (3) and (4), where F_2 is the shear force applied by digital force gauge 2, f denotes the static friction between the metal jig and the sensor surface, f′ is the static friction between the metal jig and the pushing jig, and F_S is the shear force applied to the sensor.

$$F_2 = f + f' \tag{3}$$

$$F_S = f = F_2 - f' \tag{4}$$

It is possible to sandwich a material such as urethane foam between the metal jig and the sensor so that the frictional force can be increased to more definitively apply shear force to the sensor. However, it should be noted that the actual applied shear force would be slightly smaller than the gauge value in that case. Considering static friction f′ on the upper part of the metal jig, the shear force F_S applied to the sensor can be maximized by inserting a sheet with very low friction or setting the three-axis robot to follow the shearing movement.

After evaluating the basic performance of shear force sensing using the experimental setup described above, we verified the shearing force applied to the sensor when lifting the weight using a two-finger gripper and a robot arm (UR5, Universal Robots). As shown in Figure 11(a), the jig with the weight suspended is sandwiched between two types of sensors using the two-finger gripper. I-Scan [24] is a commercially available pressure sensor that is used for continuous monitoring of the vertical force (F_1) that is applied by the two-finger gripper as a reference in this experiment. The applied vertical force, F_1, is 76 kPa. Here, assuming that the robot hand lifts a smartphone or a water bottle, we tested the shear forces of 0.15 kg and 0.65 kg. When the robot arm moves upward, a load formed by the weight is applied to the jig, and subsequently a 1.47 N and 6.37 N of shearing force is applied to the sensor as shown in Figure 11(b). The four graphs show the time decay of the output voltage when the shear force is applied in the downward direction in Figure 11(c) and in the diagonal 45° direction in Figure 11(d). To clearly indicate the direction in which the shearing force was applied, the difference between the output voltages in the x- and y- directions, ΔV_x and ΔV_y, are shown in the graph. As expected, when shear force was applied in the downward direction, ΔV_y started to decrease, whereas ΔV_x showed no change. In contrast, when shear force was applied in the diagonal 45° direction, ΔV_y decreased and ΔV_x increased in a nearly symmetrical shape. Sufficient signal could not be obtained with a shearing force of 0.15 kg, however, it is thought that this can be improved by controlling the elastic modulus of the pressure-sensitive elastomer or by revising the circuit configuration.

V. Conclusion

After conducting an in-depth circuit simulation with experimentally obtained pressure-sensitive elastomer and LTPS TFT characteristics, 1Tr-1R type pressure sensors and 2Tr-4R type shear-force sensors were fabricated on a glass-based LTPS TFT backplane. The basic performance of the pressure sensor was evaluated. It was confirmed that it is possible to accurately detect a wide range of pressures and that it shows excellent object recognition performance that exceeds that of the human finger. Furthermore, we proposed a new type of shear-force sensor, thin and not bulky, which is completely different from previously reported shear-force sensors. We then validated the practical use of lifting the weight using a robot arm.

We obtained reasonable results showing that the sensor could indicate the shearing direction from the output signal.

Because this sensor is an LTPS-based technology that has already been widely applied, it will be possible in the future to integrate various functions, such as pressure sensors, shear sensors, and temperature sensors, and to fabricate it on a flexible substrate with a higher taxel resolution. It is a promising sensor for multifunctional robots that can perform complicated tasks.

Acknowledgment

The authors gratefully acknowledge Ichikawa's and Watanabe's previous and preparatory work from the Display Research Department, LG Japan Lab Inc. The authors would like to thank Haewon Lee, Yongchan Park, and Juhan Kim for their kind support of TFT array design and fabrication process at LG Display prototype line. They would also like to thank Dr. Yoshida, President of the LG Japan Lab Inc., for helpful discussions and comments on the manuscript. They would also like to thank Editage (www.editage.com) for English language editing.

References

[1] K. Kamiyama, K. Vlack, T. Mizota, H. Kajimoto, K. Kawakami, and S. Tachi, "Vision-based sensor for real-time measuring of surface traction fields," *IEEE Comput. Graph. Appl.*, vol. 25, no. 1, pp. 68–75, Jan. 2005.

[2] R. Li *et al.*, "Localization and manipulation of small parts using GelSight tactile sensing," in *Proc. IEEE/RSJ Int. Conf. Intell. Robots Syst. (IROS)*, Sep. 2014, pp. 3988–3993.

[3] E. Donlon, S. Dong, M. Liu, J. Li, E. Adelson, and A. Rodriguez, "GelSlim: A high-resolution, compact, robust, and calibrated tactile-sensing finger," in *Proc. IEEE/RSJ Int. Conf. Intell. Robots Syst. (IROS)*, Oct. 2018, pp. 1927–1934.

[4] A. Yamaguchi and C. G. Atkeson, "Combining finger vision and optical tactile sensing: Reducing and handling errors while cutting vegetables," in *Proc. IEEE-RAS 16th Int. Conf. Hum. Robots (Humanoids)*, Nov. 2016, pp. 1045–1051.

[5] T. Someya, T. Sekitani, S. Iba, Y. Kato, H. Kawaguchi, and T. Sakurai, "A large-area, flexible pressure sensor matrix with organic field-effect transistors for artificial skin applications," *Proc. Nat. Acad. Sci. USA*, vol. 101, no. 27, pp. 9966–9970, Jul. 2004.

[6] T. Someya *et al.*, "Conformable, flexible, large-area networks of pressure and thermal sensors with organic transistor active matrixes," *Proc. Nat. Acad. Sci. USA*, vol. 102, no. 35, pp. 12321–12325, 2005.

[7] F. Jiang, G.-B. Lee, Y.-C. Tai, and C.-M. Ho, "A flexible micromachine-based shear-stress sensor array and its application to separation-point detection," *Sens. Actuators A, Phys.*, vol. 79, no. 3, pp. 194–203, Feb. 2000.

[8] K. Noda, K. Hoshino, K. Matsumoto, and I. Shimoyama, "A shear stress sensor for tactile sensing with the piezoresistive cantilever standing in elastic material," *Sens. Actuators A, Phys.*, vol. 127, no. 2, pp. 295–301, Mar. 2006.

[9] E.-S. Hwang, J.-H. Seo, and Y.-J. Kim, "A polymer-based flexible tactile sensor for both normal and shear load detections and its application for robotics," *J. Microelectromech. Syst.*, vol. 16, no. 3, pp. 556–563, Jun. 2007.

[10] C.-C. Wen and W. Fang, "Tuning the sensing range and sensitivity of three axes tactile sensors using the polymer composite membrane," *Sens. Actuators A, Phys.*, vols. 145–146, pp. 14–22, Jul. 2008.

[11] L.-T. Chen, J.-S. Chang, C.-Y. Hsu, and W.-H. Cheng, "Fabrication and performance of MEMS-based pressure sensor packages using patterned ultra-thick photoresists," *Sensors*, vol. 9, no. 8, pp. 6200–6218, Aug. 2009.

[12] H. Oh, G.-C. Yi, M. Yip, and S. A. Dayeh, "Scalable tactile sensor arrays on flexible substrates with high spatiotemporal resolution enabling slip and grip for closed-loop robotics," *Sci. Adv.*, vol. 6, no. 46, Nov. 2020, Art. no. eabd7795.

[13] J. G. Rocha, C. Santos, J. M. Cabral, and S. Lanceros-Mendez, "3 axis capacitive tactile sensor and readout electronics," in *Proc. IEEE Int. Symp. Ind. Electron.*, vol. 4, Jul. 2006, pp. 2767–2772.

[14] H. K. Lee, J. Chung, S. I. Chang, and E. Yoon, "Normal and shear force measurement using a flexible polymer tactile sensor with embedded multiple capacitors," *J. Microeletromech. Syst.*, vol. 17, no. 4, pp. 934–942, 2008.

[15] W.-Y. Chang, T.-H. Fang, S.-H. Yeh, and Y.-C. Lin, "Flexible electronics sensors for tactile multi-touching," *Sensors*, vol. 9, no. 2, pp. 1188–1203, 2009.

[16] M.-Y. Cheng, C.-L. Lin, Y.-T. Lai, and Y.-J. Yang, "A polymer-based capacitive sensing array for normal and shear force measurement," *Sensors*, vol. 10, no. 11, pp. 10211–10225, Nov. 2010.

[17] F. Ansari and Y. Libo, "Mechanics of bond and interface shear transfer in optical fiber sensors," *J. Eng. Mech.*, vol. 124, no. 4, pp. 385–394, Apr. 1998.

[18] M. Ohka, H. Kobayashi, and Y. Mitsuya, "Sensing characteristics of an optical three-axis tactile sensor mounted on a multi-fingered robotic hand," in *Proc. IEEE/RSJ Int. Conf. Intell. Robots Syst.*, Aug. 2005, pp. 493–498.

[19] X. Zhao *et al.*, "A nano-opto-mechanical pressure sensor via ring resonator," *Opt. Exp.*, vol. 20, no. 8, pp. 8535–8542, Apr. 2012.

[20] Silvaco. *SmartSpice*. Accessed: Dec. 27, 2021. [Online]. Available: https://silvaco.com/spice-simulation/parallel-spice-simulator/

[21] D. N. Nahar, S. Shafie, A. Mardhiyah, M. N. Hamidon, and F. Ahmad, "Analysis of resistive type pressure sensors for static calibration," in *Proc. IEEE 5th Int. Conf. Smart Instrum., Meas. Appl. (ICSIMA)*, Nov. 2018, pp. 1–4.

[22] H. Liu, Y. Wu, F. Sun, and D. Guo, "Recent progress on tactile object recognition," *J. Adv. Robot. Syst.*, vol. 14, no. 4, pp. 1–12, Jul. 2017.

[23] J. Tong, O. Mao, and D. Goldreich, "Two-point orientation discrimination versus the traditional two-point test for tactile spatial acuity assessment," *Frontiers Hum. Neurosci.*, vol. 7, pp. 1–11, Sep. 2013.

[24] Tekscan. *I-Scan*. Accessed: Dec. 27, 2021. [Online]. Available: https://www.tekscan.com/products-solutions/systems/i-scan-system

Noriyuki Kawashima received the B.E. degree in material engineering from Kyoto University in 1996 and the M.E. degree in material engineering from the University of Tokyo in 1998. He has been researching LTPS TFT and organic TFT (OTFT) for flexible display applications. His current research interests include tactile/shear-force sensors and actuators.

Tomohiro Sampei received the B.E. degree in material engineering from the Shibaura Institute of Technology in 2002. His research interests include LED device assembly and tactile sensors.

Takuro Tanaka received the B.S. and M.S. degrees in physics from Nagoya University in 2007 and 2009, respectively. His research interests include magnetic materials, spintronics, and machine learning.

Daiki Suzuki received the B.S. and M.S. degrees in material and biological chemistry from Yamagata University in 2014 and 2016, respectively. His research interests include smell sensors and tactile sensors.

Kazunori Morita received the B.E. degree in electronic engineering from the Hiroshima Institute of Technology in 2001. His research interests include circuit design of LCD, wearable devices, and tactile sensors.

Miya Yoshimoto received the B.S. and M.S. degrees in material science and technology from the Tokyo University of Science in 2012 and 2014, respectively. Her research interest includes biomarker nanoparticles.

Katsuyoshi Hiraki received the B.E. degree in electrical and computer engineering from Kanazawa University in 1997. His research interests include circuit design of LCD, touch panel devices, and tactile sensors.